ARTICLE

A Computational Descriptor Analysis on Excited State Behaviours of a Series of TADF and Non-TADF Compounds

Pelin Ulukan,[a] Ekin Esme Bas,[a] Rengin Busra Ozek,[a] Cansul Dal Kaynak,[a] Antonio Monari,[b,c] Viktorya Aviyente*,[a] and Saron Catak *,[a]

The thermally activated delayed fluorescence (TADF) behaviours of seventeen organic TADF emitters and two non-TADF chromophores bearing various donor and acceptor moieties were investigated, focusing on their torsion angles, singlet-triplet gap (ΔEST), spin orbit couplings (SOC) and topological Φ_S index. Electronic structure calculations were performed in the framework of the Tamm-Dancoff approximation (TDA) allowing to characterize the possible reverse intersystem crossing pathways (RISC) pathways. The electronic density reorganization of the excited states was checked also with respect to the different exchange-correlation functional and absorption spectra were obtained by considering vibrational and dynamical effects through a Wigner sampling of the ground state equilibrium regions. Examining all the parameters obtained in our computational study, we rationalized the influence of electron-donating and electron-accepting groups and the effects of geometrical factors, especially torsion angles, on a wide class of diverse compounds ultimately providing an easy and computationally effective protocol to assess TADF efficiencies.

Introduction

Since the original proposal of Organic Light-Emitting Diodes (OLEDs) by Tang and Van Slyke in 1987,[1] significant progresses have been achieved in their development and application in different technologies, including display apparatus. OLEDs represent an important innovation in lighting markets, providing improved image quality, high brightness, low fabrication costs, low power consumption and high durability.[2,3] They operate based on the physical phenomenon known as electroluminescence (EL), i.e. the conversion of electrical energy into light.[4] In OLEDs, EL is achieved by fluorescent materials, which undergo a two-step process, an initial absorption leading to the population of an electronically excited state and a subsequent radiative decay to the electronic ground state, which is known as prompt fluorescence.[2] However, despite possessing useful properties, several drawbacks still limit the development of OLEDs, notably related to technical issues, such as high-power consumption, insufficient device efficiency, and high driving voltage. Insufficient device efficiencies in OLEDs, has led to the use of high quantum yield phosphorescent materials utilizing alternative routes to achieve radiative decay. These are based on intersystem crossing (ISC), and hence the population of triplet states, leading to phosphorescence.[5] The exploitation of both singlet and triplet excited states has led to an increase in internal quantum efficiencies (IQE) up to 100%. Although the use of phosphorescent materials significantly raised quantum efficiencies in OLEDs, the use of heavy metals, such as Ir or Pt, limited their application due to increased device costs, environmental pollution, and toxicity. Moreover, the lack of stability is an additional drawback of phosphorescent OLEDs (PhOLEDs). Indeed, chemical degradation

leading to charge traps, non-radiative recombination sites, and luminance loss, are serious issues affecting PhOLEDs.[5] In the quest to increase OLED efficiencies, thermally activated delayed fluorescence (TADF) materials have attracted great attention as they lead to the population of both singlet and triplet states without using any heavy metals (Figure 1).[6–12]

Soon after the first organic TADF emitter was reported in 2011, studies related to TADF based OLEDs gained momentum and nowadays, external quantum efficiencies (EQE) reaching up to 30% together with internal quantum efficiencies (IQE) of 100% have been reported.[13] In addition to their applications in OLEDs, TADF materials also have applications in fluorescence lifetime imaging,[14] and oxygen sensing. [15 -16]

TADF materials also possess the critical advantage of enabling different colour emission[20–34] and serving as host materials in emission layers.[30] Emission, which may span from blue to red, is mainly controlled by the degree of intramolecular charge transfer (ICT) of the involved excited states.[31-32] Since ICT is one of the most important parameters in TADF activity, numerous design strategies were attempted to enhance this fundamental process. One strategy involves the use of donor–acceptor (D-A), D-π-A, D-π-A-π-D molecular frameworks, in which the highest occupied molecular orbitals (HOMO) and lowest unoccupied molecular orbital (LUMO) are localized on donor and acceptor units, respectively, hence leading to spatially separated frontier orbitals.[33] Various donor and acceptor groups were designed to enhance charge transfer in TADF luminophores. The most frequently used donor moieties are diphenylamine,[2,34,35] carbazole,[23,36–44] acridine,[17,20,45] and phenoxazine derivatives,[46–49] while the most common acceptor units include boron,[50–58] sulfone,[23,25,41] and benzophenone derivatives (Figure 2).[20,24,59,60] However, TADF systems are not limited to these building blocks, other interesting frameworks were designed such as cyanobenzenes,[59] triazines,[61] oxadiazoles,[31] sulfones,[62] and spiro derivatives.[63,64]
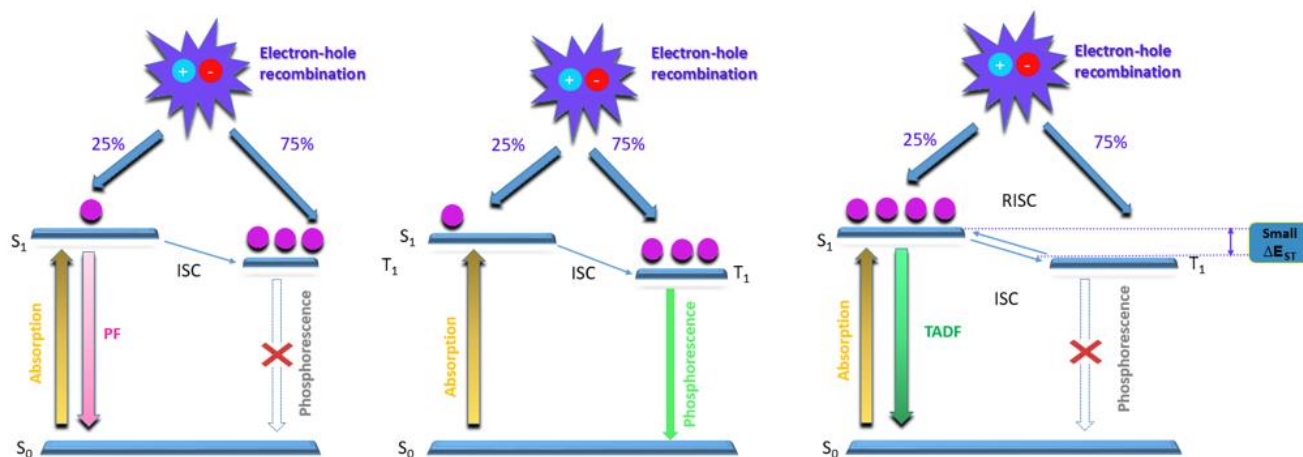
ARTICLE

Figure 1. Jablonski diagram for OLED, PHOLED and TADF materials, respectively.

From a photophysical point of view, TADF is based on the up conversion from the triplet (T_1) to the singlet (S_1) state, which is only possible if ΔE_{ST} is sufficiently small, i.e. less than 0.1 eV. Such an energetic alignment facilitates the reverse intersystem crossing process (RISC), which is also known as up-intersystem crossing process (UISC).[65] Although TADF compounds with ΔE_{ST} values smaller than 0.1 eV show the best performances, some fluorophores with ΔE_{ST} values close to 0.5 eV exhibit TADF emission. However, though TADF mechanism usually involves RISC between T_1 and S_1 states, an alternative possible pathway driven by higher excited triplet states is also observed. Indeed, in some circumstances more than one triplet states are present below the S_1 state, allowing reverse internal conversion (RIC) between T_1 and the upper lying triplet states. This is followed by a RISC between T_n, i.e. the triplet state closest to the first excited singlet state and and S_1.[66] Furthermore, rigid molecular architectures are usually preferred over flexible ones for high performance TADF devices, since they minimize non-radiative decay due to vibrational and rotational motions.[67] In addition to a small ΔE_{ST} gap, the electronic coupling between charge transfer singlet (^1CT) and local triplet (^3LE) states strongly influences TADF efficiency.[68] Indeed, the magnitude of spin orbit coupling (SOC) is crucial to determine RISC efficiency and ultimately delayed fluorescence.[69]
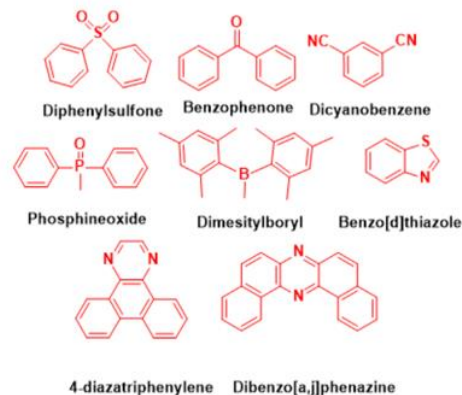
The rate of RISC (k_{RISC}) is usually expressed combining Fermi's Golden Rule with Marcus' Theory, [70] as:

$$k_{RISC} = \frac{2\pi}{\hbar}|H_{SO}|^2(4\pi\lambda k_B T)^{-\frac{1}{2}}\exp\left(\frac{-E_A}{k_B T}\right) \quad (1)$$
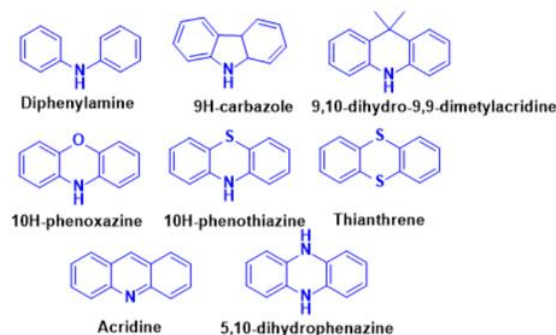
$$E_A = \frac{(\Delta E_{ST} + \lambda)^2}{4\lambda} \quad (2)$$

The key parameters being the reorganization energy λ, the SOC expressed by H_{SO}, and E_a which is related to the ΔE_{ST} energy gap through equation 2.

Figure 2. Commonly used acceptor (red) and donor (blue) moieties in TADF molecules.[71]

More topological descriptors of the electronic density reorganization such as the amount of CT (q^{CT}) and the effective CT distance (d^{CT}) for ground and excited states have also been used to computationally preview TADF performance.[72] The CT character of T_1 states has also been analyzed through the excited state dipole moments.[73] Furthermore, environmental factors are also important in dictating the overall TADF efficiency, in particular the ISC rates, as shown by their sensitivity to solvent polarity.[65]

In addition, as Yu-Zhong Xie and co-workers pointed out, minimum energy crossing points (MECP) between S_1 and T_1 states are crucial, since they represent funneling regions, allowing the non-adiabatic transition between different electronic states.[74]

In our previous study, we investigated a series of benzophenone based TADF emitters and non-TADF chromophores by quantum chemical calculations. Our main goal in that contribution was to understand the photophysical properties of benzophenone emitters and their derivatives in terms of absorption spectra, charge separations in the excited states, ΔE_{ST} gaps and SOC magnitude.[75] Here, on the other hand, we plan to extend the objectives of the previous study investigating TADF emitters with various acceptor moieties and propose a new a more general computational strategy applicable to a large variety of TADF emitters. For this purpose, we analyzed the relationship between molecular structures and photophysical properties of a wide range of emitters by means of *ab initio* calculations. To understand the correlation between the molecular structure and TADF properties, a comparative study is performed along molecules that possess TADF features and compounds known to be poor TADF emitters (henceforth, they will be referred to as non-TADF molecules). Indeed, a systematic study on the relation between structural, electronic properties, and the TADF efficiency of different classes of compounds is somehow missing. We plan to bridge this gap by using molecular modelling and simulation to provide a unified description of the different parameters related to TADF performance.

For this purpose, ground state structural properties, such as the torsional angles, are explored and related to the optical properties and the singlet-triplet gap. Our analysis of different excited state descriptors, including singlet-triplet gap, SOC magnitude, and the amount of charge transfer provides a useful and computationally effective protocol to rationalize TADF efficiency.

Although the RISC probability decreases with the increase in ΔE_{ST}, H_{SO} which competes with ΔE_{ST}, albeit being usually overlooked, may play a significant role and hence, should be properly accounted to sketch useful design rules for TADF compounds.

Computational Methodology

Prior to the evaluation of all optical and photophysical properties, a conformational analysis was performed using the Gaussian 16 software package[76] to characterize all possible conformers of the chosen TADF and non-TADF molecules. Density Functional Theory (DFT) calculations with the M06-2X[77,78] meta-hybrid functional and the 6-31+G(d,p)[75] basis set have been carried out to optimize the ground state conformers and the corresponding S_1 and T_1 geometries. However, all conformers are expected to share the same TDA behavior since the latter is mainly dictated by the twisting angle between donor and acceptor moieties or between the donor and bridge moieties, which are highly conserved in the conformational space. While for ground state equilibrium geometries we have checked that no imaginary vibrational frequencies are present, this was not performed for S_1 and T_1 equilibrium geometries due to the lack of analytical hessians. The choice of M06-2X functional is

justified by its good performance in reproducing the geometries of aromatic compounds.[79] In our previous study, the excited state properties obtained by taking into account all the possible conformers of TADF molecules have been proven identical to the ones of the lowest energy conformer.[75] Thus, we continue our analysis considering the lowest energy conformers of each molecule, only (see Tables S1-S5). The energy and nature of excited states are assessed at the B3LYP[80]/6-31+G(d,p), M06-2X/6-31+G(d,p), CAM-B3LYP[81]/6-31+G(d,p), wB97XD[82]/6-31+G(d,p) levels of theory, 6-311++G(3df,3pd)[83] and 6-311++G(2d,2p)[84] basis sets were used, in all calculations, for sulfur and phosphorus atoms, respectively. A series of benchmark calculations with Becke's hybrid B3LYP functional and 6-31+G(d,p) and 6-311+G(d,p) basis sets are also performed. From this test, it is clearly observed that increasing the basis set does not induce any noticeable change on the calculated absorption spectra (see Tables S6-S7).

Integral equation formalism polarizable continuum model (IEF-PCM) is used in all calculations,[85] to implicitly model the solvent environment. Optimized geometries were rendered with CYLview software package.[86]

Tamm Dancoff Approximation (TDA) was employed for all the excited state calculations. This choice is due to the fact that the TDA method provides a more balanced description of both triplet and singlet excited states, and compared to Time-Dependent DFT (TD-DFT) is free from triplet instability issues.[87] All excited state calculations have been carried out with the Gaussian 16 software package. Absorption spectra were modeled as vertical transitions from the S_0 equilibrium geometry. Subsequently, to include dynamic and vibrational effects, 30 conformations, sampling the vicinity of the Frack-Condon region, were generated through a Wigner distribution[88] as implemented in the Newton-X[89] software package. Vertical transitions from each snapshot were convoluted using Gaussian functions of full-width at half length (FWHL) of 0.15 eV. Absorption spectra calculations via Wigner distribution method have been performed with B3LYP, PBE0, M062X, BLYP[90] and TPSSh[91] functionals using the 6-31+G(d,p) basis set.

The nature of the excited states is evaluated using Natural Transition Orbitals (NTOs), obtained with the Nancy_EX code[92,93] and visualized with the Avogadro[94] software package. In addition, Φ_S values, defining the overlap between the attachment and the detachment densities, were calculated. Spin-orbit couplings (SOC) between S_1 and T_1 states have been calculated at the TDA level by using the Amsterdam Density Functional (ADF) code[95,96] at the B3LYP/DZP[97] and M06-2X/DZP levels of theory. DZP was used since Pople basis sets are not available in ADF.

Results and Discussion

Herein, a series of different TADF emitters with various donor and acceptor groups were selected from the literature and were investigated by TDA-DFT methods (see Figure 3). In an attempt to identify the presence of TADF characteristics in the selected emitters, several descriptors were assessed, such as the twisting angle between donor and acceptor units, ΔE_{ST}, NTO densities along with the charge transfer topology indices (Φ_S),[98] and SOC values between the S_1 and T_n states involved in the RISC process.

We selected TADF compounds containing different acceptor groups, such as phosphine oxides, phenazines, anthraquinones, phenanthrenes, diphenylsulfones and benzophenones. Specifically, we consider the phosphine oxide (PX-ZPO, DPX-ZPO and TPX-ZPO[99]), dibenzo[a,j] phenazine (MeODP-DBPHZ, POZ-DBPHZ[100]), anthraquinone-based compounds (AQ-DMAC, AQ-DPA),[101]

ARTICLE
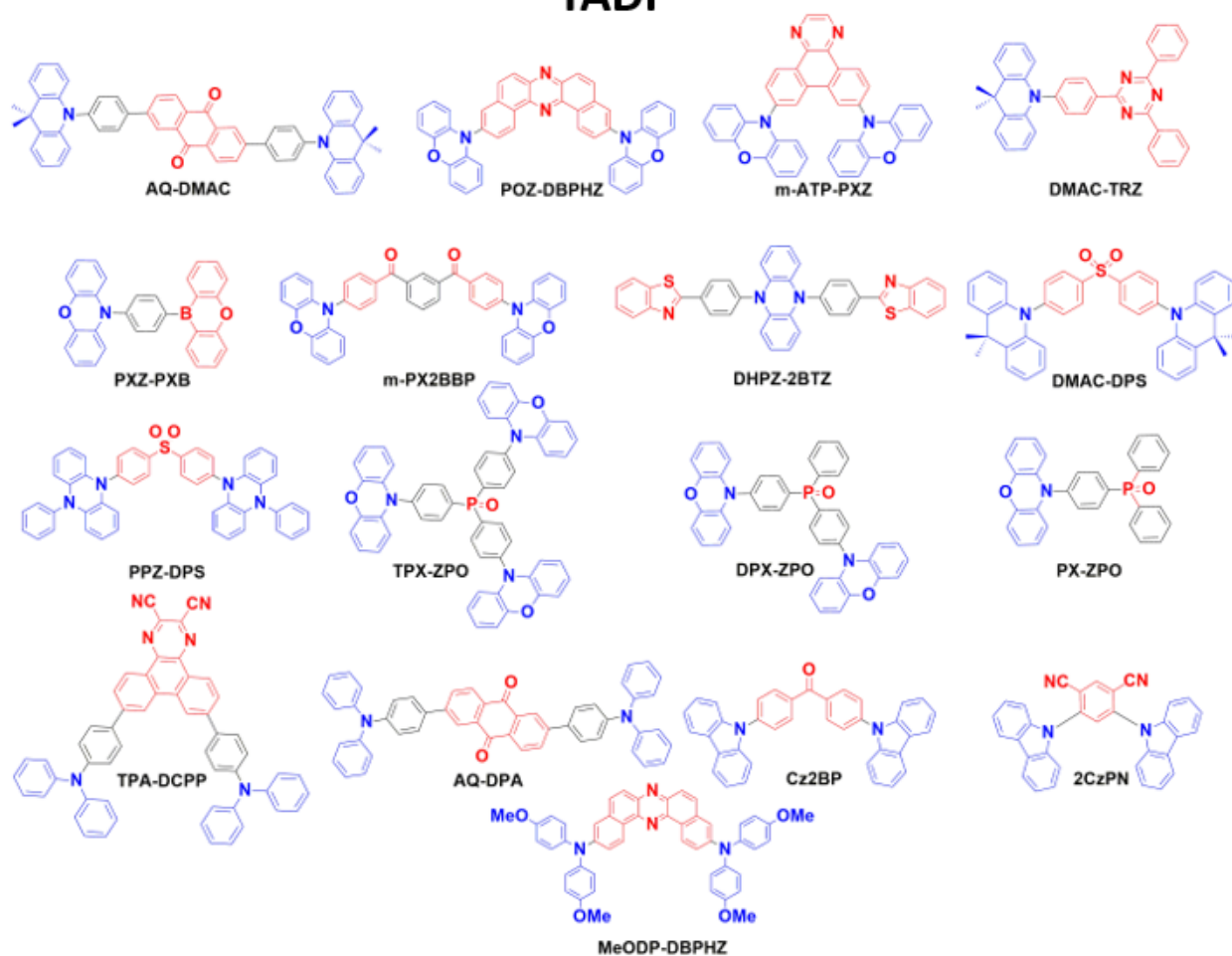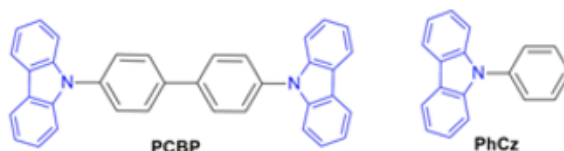
TADF

NON-TADF

Figure 3. TADF and non-TADF molecules investigated in this study. Blue color represents donor and, red color represents acceptor moieties. Black colored groups are used as π-bridges.

phenanthrene containing compounds (m-ATP-PXZ[102], TPA-DCPP[103]) diphenylsulfone-based compounds (DMAC-DPS, PPZ-DPS)[104] and benzophenone containing compounds (m-PX2BBP and Cz2BP)[105] Additionally, we studied PXZ-PXB bearing a 10H-phenoxaboryl electron acceptor group,[106] DMAC-TRZ with 2,4,6-triphenyl-1,3,5-triazine (TRZ) acceptor moiety,[107] and 2CzPN with dicyanobenzene group.[108] Furthermore, and as a comparison, we also considered two non-TADF molecules namely, pCBP and PhCz.[109]

Twist Angle Between Donor (D), Acceptor (A) and Bridge (B) Moieties

The torsion angle between donor/acceptor units and the bridge moieties is a straightforward descriptor allowing to rationalize the TADF activity, and the calculated values are reported in Figure 4. As a matter of fact, twisting angles of 90° will constitute the perfect arrangement to break conjugation, thus leading to small ΔE_{ST} values and, hence, enhance TADF. However, while minimizing ΔE_{ST} values,

perfectly orthogonal geometries lead to an important disadvantage for luminescence, since the oscillator strengths, which is one of the key parameter for light emission, is then strongly reduced. Among seven different donor units we show that the best performing group is clearly DMAC with its ~90° twisting, while PXZ moiety with ~80° twist angle is the second most efficient donor group.
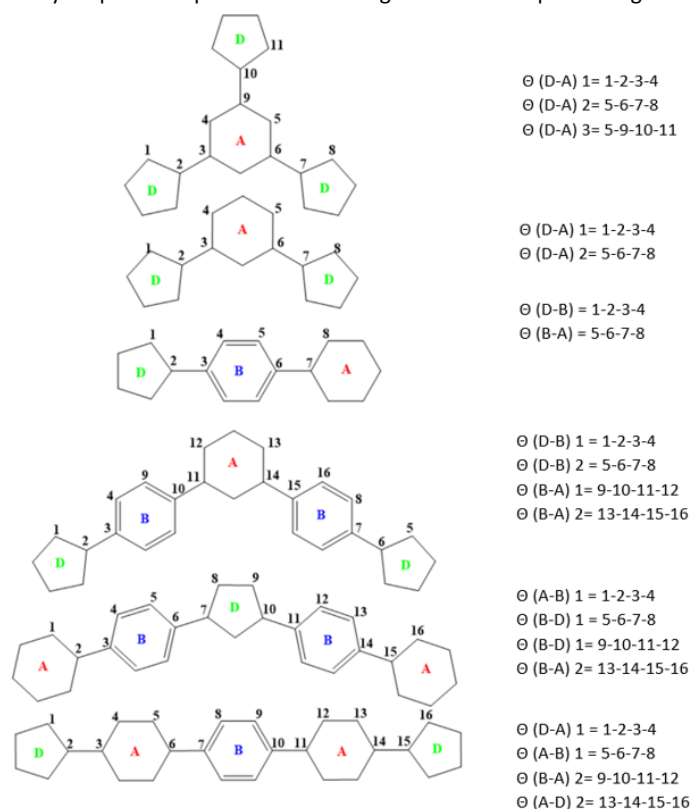
As expected, the favorable value of the twist angle is reflected in PXZ-containing compounds which present small ΔE_{ST} values, as seen both experimentally and theoretically (Figure S2). PPZ and DHPZ display a twisting of ~100° between the adjacent neighboring groups. These structural features also correlate with ideal ΔE_{ST} values (<0.1 eV) and well separated frontier orbitals as can be seen from Figure S3. On the contrary, TPA-DCPP, AQ-DPA and MeODP display relatively lower TADF activity due to their small twist angle, which are close to 30°. The small twisting can be attributed to the freely rotating phenyl rings, which cause a general planarization of the compounds. The last donor unit, Cz, induces a torsion angle of around 50°-60°. The relatively low torsion angle of the carbazole moiety can be attributed to a smaller steric repulsion due to the five-membered ring in the donor group. In addition to the torsion angles between donor and adjacent moieties, we also examined the twisting angles between acceptor units and their adjacent donor or bridge moieties (Figure 4). While the triphenyl triazine acceptor induces a twisting angle of 90°, DBPHZ and m-ATP units reach approximately 80°.

On the other hand, the DPS moiety leads to an ideal 90° twisting with DMAC and 100° angle with PPZ group. Instead, relatively low performance TADF emitters, such as Cz2BP and 2CzPN, assume a butterfly shape. Benzophenone-containing TADF emitters presenting a D-A-D scaffold, reach twist angles of ~52° and ~120° thus leading to a non-orthogonal geometry. Indeed, also due to its efficient ISC, benzophenone was previously explored as an OLED emitter.[59]

In addition to the Franck-Condon region, the torsion angles at the equilibrium T_1 geometries were also examined, and, as reported in Table 1, only slight changes can be observed except for compound 7. Moreover, torsion angles at the S_1 equilibrium geometries were also obtained for AQ-DMAC, POZ-DBPHZ, DHPZ-2BTZ, PPZ-DPS, Cz2BP, TPA-DCPP, AQ-DPA and MeODP-DBPHZ. It has been observed that equilibrium geometries for the first excited singlet state are very close to those of the ground state. Therefore, to reduce computational costs, further analyses have been performed at Franck-Condon region, only. Thus, geometry relaxation is important only for the T_1 state, leading to a decrease in orthogonality, and consequently to the increase of the HOMO-LUMO overlap and ΔE_{ST}. Indeed, excited state twisting is recognized as a key feature of TADF molecules.

To sum up, DMAC, PXZ and DHPZ units appear as the most appropriate donors to establish the desired orthogonality leading to twisting angles around 80° and 100°. On the other hand, DPA derivatives have smaller twisting angles (~40°), which lead to increased HOMO-LUMO overlap and ΔE_{ST}. Moreover, when considering acceptor moieties, anthraquinone and diphenylsulfone groups provide almost ideal orthogonal arrangements. It should be pointed out, however, that the term ideal here refers to geometrical properties and twisting angle only and not to the device performance.

$\ominus$ (D-A) 1= 1-2-3-4
$\ominus$ (D-A) 2= 5-6-7-8
$\ominus$ (D-A) 3= 5-9-10-11

$\ominus$ (D-A) 1= 1-2-3-4
$\ominus$ (D-A) 2= 5-6-7-8

$\ominus$ (D-B) = 1-2-3-4
$\ominus$ (B-A) = 5-6-7-8

$\ominus$ (D-B) 1 = 1-2-3-4
$\ominus$ (D-B) 2 = 5-6-7-8
$\ominus$ (B-A) 1= 9-10-11-12
$\ominus$ (B-A) 2= 13-14-15-16

$\ominus$ (A-B) 1 = 1-2-3-4
$\ominus$ (D-B) 1 = 5-6-7-8
$\ominus$ (B-D) 1= 9-10-11-12
$\ominus$ (B-A) 2= 13-14-15-16

$\ominus$ (D-A) 1 = 1-2-3-4
$\ominus$ (A-B) 1 = 5-6-7-8
$\ominus$ (B-A) 2= 9-10-11-12
$\ominus$ (A-D) 2= 13-14-15-16

D-A	θ(D-A)1	θ(D-A)2	θ(D-A)3
DMAC-TRZ	89.50	-	-
TPX-ZPO	-103.6	9.85	-76.01
DPX-ZPO	-103.62	-75.74	-
PX-ZPO	76.76	-	-
D-A-D	**θ(D-A)1**	**θ(D-A)2**	
POZ-DBPHZ	77.89	-104.66	
M-ATP-PXZ	77.44	77.39	
MeODP-DBPHZ	25.32	-27.27	
DMAC-DPS	-91.08	89.23	
PPZ-DPS	-103.56	102.96	
Cz2BP	51.43	51.43	
2CzPN	119.78	-59.80	
D-B-A	**θ(D-B)1**	**θ(B-A)2**	
PXZ-PXB	-78.74	53.94	

D-B-A-B-D	θ(D-B)1	θ(A-B)1	θ(A-B)2	θ(D-B)2
AQ-DMAC	89.39	-38.44	38.45	-89.26
TPA-DCPP	-34.98	-37.01	-36.93	-35.40
AQ-DPA	-35.84	-36.21	35.71	-36.20
A-B-D-B-A	**θ(A-B)1**	**θ(B-D)1**	**θ(B-D)2**	**θ(A-B)2**
DHPZ-2BTZ	0.00	102.18	102.18	0.00
D-A-B-A-D	**θ(D-A)1**	**θ(A-B)1**	**θ(A-B)2**	**θ(D-A)2**
m-PX2BBP	75.44	-30.90	-30.98	75.45
Non-TADF	**θ(D-B)1**	**θ(B1-B2)**	**θ(D-B)2**	
PCBP	-55.44	37.55	-55.45	
PhCz	-55.89			

Figure 4. Ground State Twist angles of TADF and Non-TADF molecules. D: Donor unit, A: Acceptor unit, B: Bridge unit.

Table 1. 3D representations of S_0 and T_1 geometries of some compounds with different ground state and excited state geometries and changes in torsion angles (M06-2X/6-31+G(d,p) level of theory).

	S_0	T_1		S_0	T_1
DMAC-TRZ (1)			POZ-DBPHZ (2)		
m-ATP-PXZ (3)			MeoDP-DBPHZ (4)		
DMAC-DPS (5)			PPZ-DPS (6)		
2CzPN (7)			PXZ-PXB (8)		

S_0/T_1 Geometries Torsion Angles

|	θ(D-A)1	θ(D-A)2		
1	89.5/63.62			
	θ(D-A)1	θ(D-A)2		
2	77.89/-69.93	-104.7/-103.4		
3	77.44/75.74	77.39/66.03		
4	25.32/29.27	-27.27/-30.34		
5	-91.08/71.68	89.23/71.68		
6	-103.56/-101.8	102.96/95.49		
7	119.78/-56.63	-59.8/-56.63		
	θ(D-B)1	θ(D-B)2		
8	-78.74/69.19	53.94/37.06		
	θ(D-B)1	θ(A-B)1	θ(A-B)2	θ(D-B)2
9	-34.98/-29.33	-37.01/-27.72	-36.93/-27.72	-35.4/-29.33
10	-35.84/-41.52	-36.21/35.79	35.71/-15.04	-36.2/-24.47
	θ(A-B)1	θ(B-D)1	θ(B-D)2	θ(A-B)2
11	0/0	102.18/-90.34	102.18/90.24	0

TPA-DCPP (9)

AQ-DPA (10)

DHPZ-2BTZ (11)

ARTICLE

Electronic Density Reorganization and Effect of the Functional

The reorganization of the electronic density due to the excited state population has been analyzed examining the behavior of the corresponding NTOs. Furthermore, we compare the natures of S_1 and T_1 states obtained using M06-2X, CAM-B3LYP and ωB97XD to assess the influence of the exchange-correlation functional in the topology of the electron density reorganization (Table S8), and hence, in providing the correct diabatic description of the most relevant states.

In this respect, B3LYP functional was excluded, since TADF compounds rely heavily on CT, exasperating the known deficiencies of hybrid functionals, especially for bridged compounds leading to spatially long-range CT states.[110] Since the molecular set under investigation is composed of mostly donor-π-acceptor charge transfer molecules, we did a benchmark study with medium-range separated M06-2X and long range separated CAM-B3LYP and wB97XD functionals. Though slightly unsatisfactorily performances of CAM-B3LYP and wB97XD have been reported for some donor-acceptor systems,[111] their behavior was not tested for the set of molecules under investigation, which are typical donor-π-acceptor systems.

Table 2 reports the Φ_S values of S_1 states computed with M06-2X, ωB97XD and CAM-B3LYP functionals, while the corresponding NTO densities are reported in Figure S3. High Φ_S values indicate large overlap between electron and hole densities, thus, LE character. On the other hand, small Φ_S values indicate that the degree of overlap between electron and hole densities are small, and thus the presence of a CT excited state.

S_1 states computed with M06-2X functional mostly present a noticeable CT character, which is known to favor TADF efficiency. Conversely, CAM-B3LYP and ωB97XD functionals preview a locally excited S_1 state for some TADF compounds. Also taking into account the orthogonal arrangement, which should indeed favor charge separation, it appears that LE character should be regarded as an artifact as opposed to the more reliable M062X results (Table 3, see SI Table S8 and S12 for full list). Hence, M062X will be consistently used hereafter.
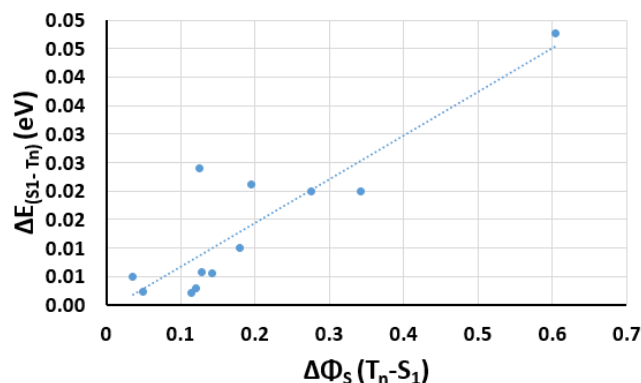
Figure 5 Correlation between ΔE_{ST} and the change in electronic density reorganization computed at M062X/6-31+G(d,p) level of theory.

Figure 5 reports the correlation between the change in the degree of overlap between S_1 and T_n states and $\Delta E_{(S1-Tn)}$. We may observe that when the nature of S_1 and T_1 changes the energy gap increases. Though a linear relationship with $R^2 = 0.99$ could not be observed, a direct proportion with a positive slope has been observed. However, these should not be necessarily considered as a drawback on RISC mechanism, since due to El Sayed rule SOC between states of different character should increase.

Table 2. Phi-S values of S_1 states computed at different levels of theory and the 6-31+G(d,p) basis set.

Phi-S Values	M062X	wB97XD	CAMB3LYP
AQ-DMAC	0.310	0.511	0.479
POZ-DBPHZ	0.094	0.841	0.099
M-ATP-PXZ	0.144	0.176	0.134
PXZ-PXB	0.064	0.487	0.511
DMAC-TRZ	0.213	0.503	0.519
m-PX2BBP	0.247	0.525	0.549
DHPZ-2BTZ	0.085	0.733	0.746
PPZ-DPS	0.160	0.612	0.591
DMAC-DPS	0.201	0.550	0.564
TPX-ZPO	0.252	0.601	0.254
DPX-ZPO	0.252	0.647	0.260
PX-ZPO	0.212	0.525	0.235
TPA-DCPP	0.728	0.588	0.612
AQ-DPA	0.610	0.517	0.642
Cz2BP	0.410	0.579	0.633
2CzPN	0.599	0.567	0.584
MeODP-DBPHZ	0.739	0.483	0.514
pCBP	0.782	0.497	0.587
PhCz	0.847	0.862	0.863

Table 3. Torsion angles and natures of S_1 states with different functionals.

Compounds	Torsion Angle	M062X	CAM-B3LYP	wB97XD
		S_1	S_1	S_1
AQ-DMAC	89.39	CT	LE	CT+LE
PXZ-PXB	78.74	CT	LE	LE
DMAC-TRZ	89.50	CT	CT	CT
PPZ-DPS	103.56	CT	CT+LE	CT+LE
DMAC-DPS	91.08	CT	CT+LE	CT+LE
TPX-ZPO	103.60	CT	CT+LE	CT+LE
DPX-ZPO	103.62	CT	CT	CT+LE

Correlation between ΔE_{S1-T1} and RISC Efficiency

According to Kasha's Rule,[74] the population of high lying singlet states is followed by ultrafast internal conversion (IC) to S_1, and eventually ISC leading to the population of the triplet manifold. IC is also active on the triplet manifold, hence leading to the T_1 population. Thus, RISC from T_1 to S_1 is not the only possible pathway, indeed reverse internal conversion (RIC) between T_1 and upper lying T_n states may be possible if the former are quasi-degenerate, which in turn will open a channel for RISC between an excited T_n and S_1 states.[66,112] Globally, however, RISC will be mainly determined by the energy order of singlet and triplet states, together with their efficient couplings. Bredas et al. have shown that the separation of frontier molecular orbitals alone is not sufficient to assure TADF efficiency and pointed to the fact that other factors, including the possibility of mixed CT T_1 states with small ΔE_{ST} gap, are crucial.[112] The electron donating character of the donor moiety may also have a noticeable effect on ΔE_{ST}, with the increase of electron donation leading to its decrease. Additionally, using donor and acceptor moieties with appropriate ionization potentials and electron affinities is another key parameter in minimizing the ΔE_{ST} gap.[73]

As shown in Figure 6, the energy levels of singlet and triplet states indicate that for many compounds, more than one triplet state is lying below the S_1 level. Additionally, in some instance T_1 and T_2 states were found to be almost energetically degenerate. For some compounds, such as DHPZ-2BTZ and PPZ-DPS, a three-state degeneracy involving S_1, T_1 and T_2 is observed. Globally, all these facts may point to the fact that higher triplet states may, indeed, contribute to the RISC process.

Therefore, to identify the states responsible for RISC, the specific value of SOC should be analysed together with the energetic gaps.

Correlation between SOC and RISC Efficiency

Besides the ΔE_{ST} descriptor, we also determined the effects of structural modifications on the SOC between S_1 and T_1 states. Indeed, despite giving rise to low lying CT with negligible electron-hole overlap, orthogonal arrangement of donor and acceptor moieties may have a negative effect on SOC, hence influencing in a more subtle way the ultimate RISC rate. Although TADF compounds are generally known to have low SOC values, it is found that RISC occur on a timescale shorter than 100 ns at 300K.[112] Furthermore, LE triplet states may be involved increasing the possibility of RISC due to the El Sayed's rule.[113,114] In this context, Penfold and Monkman suggested a RISC mechanism which involves a three state degeneracy between S_{CT}, T_{CT} and T_{LE}.[115]

Herein, we computed SOC between S_1 and the first five triplet states (see Figure 8 and Table S11). As represented in Figure 7, striking differences of SOC between S_1 and different triplet states are observed. It should be pointed out that since SOC value enters the Marcus's formula directly, couplings between the states involved in RISC are highly important. Detailed analysis of Figure 7 shows that the energy gap between the singlet and triplet states with largest SOC are very close to the experimental energy gaps. In other words, we observed that the experimental ΔE_{ST} values are very close to the calculated gaps between strongly-coupled singlet and triplet states.

For instance, for AQ-DMAC, m-ATP-PXZ, DHPZ-2BTZ, and AQ-DPA, SOC between S_1 and T_3 are larger compared to all the other states, and the absolute deviations of the computed S_1-T_3 energy gaps with the experimental values are smaller than 0.05 eV. For POZ-DBPHZ, PXZ-PXB and TPX-ZPO, S_1 and T_4 have the largest SOC and their gaps deviate by less than 0.1 eV compared to the experiment.

On the other hand, for DMAC-TRZ, DPX-ZPO, PX-ZPO and 2CzPN, SOC between S_1 and T_1 states are the highest, moreover, their corresponding energy gaps deviates by approximately 0.1 eV from the experiment, suggesting a more classic scenario involving only the lowest triplet state. For DMAC-TRZ emitter, it should be pointed out that the SOC between S_1-T_2 states is larger than for S_1-T_1. However, while T_2 state is higher, and hence shows a large energy gap, T_1 is almost degenerate with S_1. Thus, when compared with the experiment, the gap between S_1 and T_1 states is of approximately 0.006 eV.

As a matter of fact, SOC appears as a more promising, and crucial descriptor in determining the states involved in RISC process. It should also be pointed out that various TADF groups are represented in our set, and in all the cases SOC was able to reliably describe the experimental efficiency, even in the presence of wide and diverse donor and acceptor groups, and in general different functional moieties.
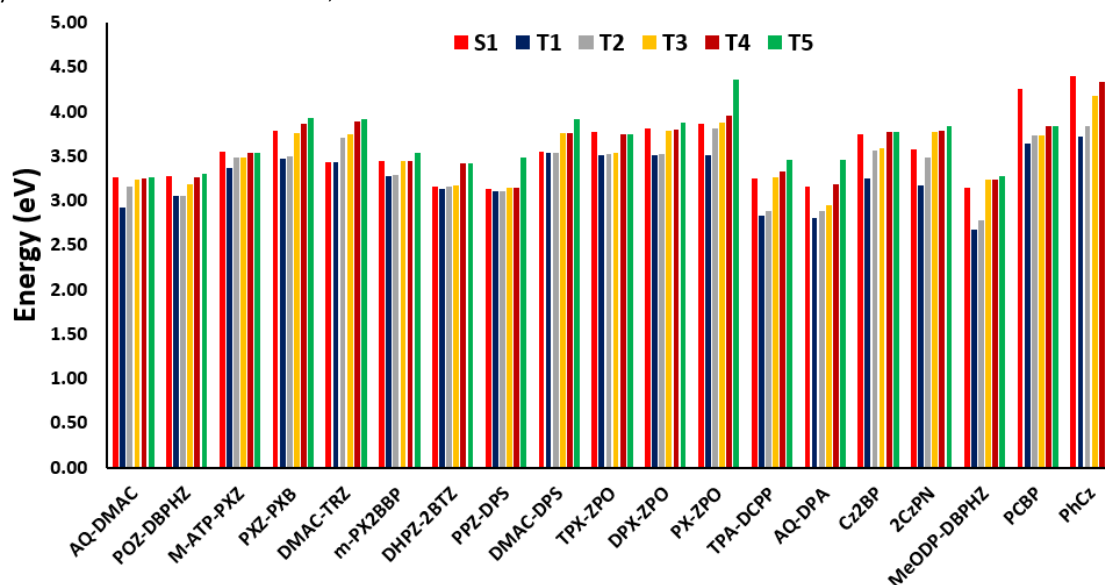
Figure 6 Energies of S_1 and T_1-T_5 levels computed at M062X/6-31+G(d,p) level of theory.

ARTICLE
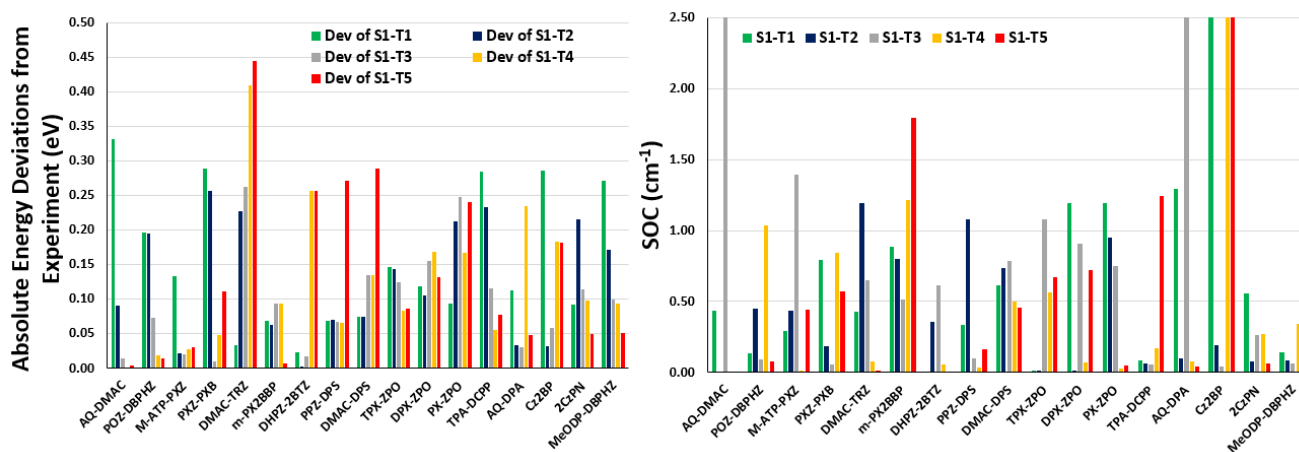
Figure 7 Absolute deviations of S-T gaps from experiment and the SOC values of computed at M062X/6-31+G(d,p) level of theory.

As a general rule, good TADF efficiency requires either moderate SOC and very small ΔE_{S1-T1} or moderate ΔE_{S1-T1} and very high SOC. Thus, almost perfectly orthogonal scaffolds including strong D and A moieties, which will result in very small ΔE_{S1-T1} and SOC values, will be less efficient than moderate strength D and A groups if they still present torsion angles leading to acceptable ΔE_{S1-T1} and strong SOC.

Another important role of SOC is its deterministic behaviour in competition between direct transition from S1 to S1 and ISC/RISC. According to the Hund's rule, T_1 state is in lower energy than the S_1 state and though both ISC and RISC processes depend on the same SOC matrix element between S_1 and T_1 states, ISC rate is always higher than RISC. Moreover, there is a competition between fluorescence emissions - ISC and generally, fluorescence emission is faster than the ISC, which is faster than the RISC process. However, in the case of TADF emitters, small singlet – triplet energy gap with localized HOMO and LUMO orbitals leads to small transition dipole for $S_1 \rightarrow S_0$ transition. Thus, due to the slow radiative rate of fluorescence caused by the small transition dipole, excited state dynamics favour the ISC to triplet states.[116]

For the molecule set under investigation, descriptors mainly ΔE_{ST} and SOC support the preference of ISC over fluorescence emission. As reported in Figure 7 and Table S11, TADF emitters under investigation exhibit strong SOC values, thus strong ISC to the triplet states. Moreover, Table S10 reports that these emitters exhibit CT character S_1 states, with localized HOMO and LUMO orbitals, thus, they are expected to have small transition dipole moments for the radiative decay between S_1 and S_0 states. Another important descriptor, ΔE_{ST}, also favors ISC over fluorescence emission, which is mainly due to the very small energy gaps between the relevant states.

Topological Φ_S Index

The Φ_S index measures the degree of overlap between particle and hole densities, and the smaller its value the larger the charge separation in the excited states. Hence, the Φ_S index can be used as an indicator for TADF efficiencies. As represented in Figure 8, going from TADF to non-TADF compounds, Φ_S indices definitely increase.

This situation is also coherent with the decrease of orthogonality and increase of ΔE_{ST}. The compounds with the smallest twisting angles between donor and acceptor units, such as Cz2BP, MeODP-DBPHZ, TPA-DCPP and AQ-DPA, or the non-TADF pCBP and PhCz present higher Φ_S indices, because of the highly delocalized π electrons, which result in hole and particle density overlap and increased LE character (Figure S3). On the other hand, compounds with higher twisting angles and lower ΔE_{ST} values exhibit lower Φ_S indices, which indicates increased CT character.[117]
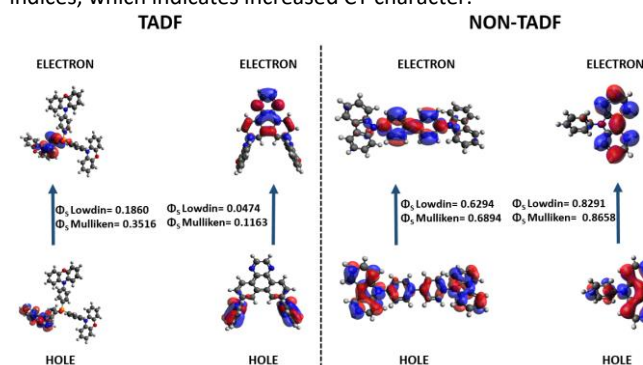
Figure 8 Φ_S indices of S_1 states and frontier molecular orbital overlap differences of TADF TPX-ZPO, m-ATPPXZ and non-TADF pCBP, PhCz molecules, respectively.

As shown in Figure 8. and Figure 9., while most of the TADF compounds have Φ_S values for S_1 smaller than 0.3, non-TADF compounds have Φ_S values close to unity. Namely this is the case for

ARTICLE
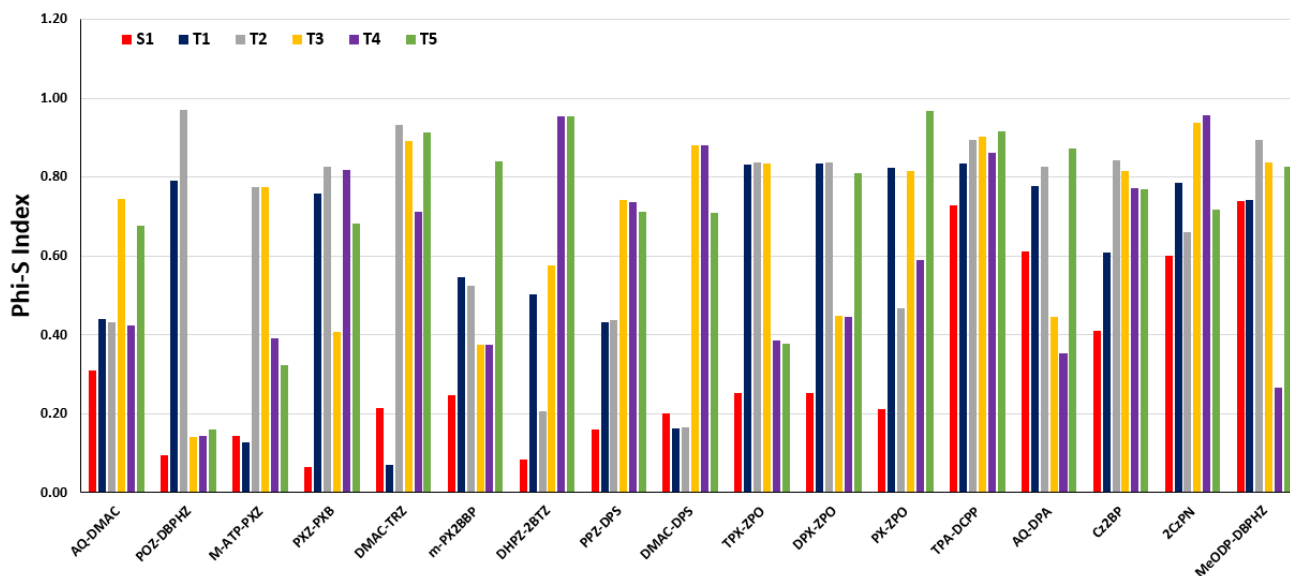
Figure 9 Phi-S indices of S_1, T_1, T_2, T_3 and T_4 states computed at M062X/6-31+G(d,p) level of theory.

TADF active MeODP, Cz2BP, TPA-DCPP, AQ-DPA and Non-TADF pCBP, PhCz. The latter also present torsion angles far from 90° and the hole and particle densities are delocalized over the conjugated bridges (Figure S3), thus justifying the high Φ_S values (see Table 2).

On the contrary, for compounds which have orthogonal D-A geometries, such as DMAC-TRZ, DMAC-DPS and AQ-DMAC, hole densities are distributed on the donor moieties while particle densities are almost perfectly localized on the acceptor groups.

In Figure 9, Φ_S indices for S_1, T_1, T_2, T_3, T_4 and T_5 states have been reported. It is obvious that while S_1 generally have CT character with small Φ_S indices, triplet states have larger Φ_S indices, thus indicating increased LE character (see Table S12 for full list of natures). Since the change in the nature of states is favorable to enhance SOC, this feature should be considered as beneficial for TADF efficiency. Moreover, when compared to Figure 6, it has been observed that energetically degenerate states such as T_3 and T_4 in AQ-DMAC have remarkable differences in their Φ_S indices, which leads to differences in their SOC values with the S_1 state. This situation is a way of obtaining strong RISC between the singlet and isoenergetic, mixed triplet states.

In summary, four main descriptors which are torsion angle, nature of states, ΔE_{ST}, Phi-S index and SOC of a series of TADF emitters were investigated with a series of benchmark calculations via TDA approximation. Here is the main findings from our benchmark study;

✓ For the nature of states analyses, PBE0, B3LYP, M06-2X, CAM-B3LYP and ωB97XD functionals with 6-31+G(d,p) basis set were used. In our calculations we observed the deficiency of hybrid functionals on modelling CT emitters. On the other hand, CAM-B3LYP and ωB97XD were found to represent LE singlet states which is not consistent with the structural properties of the TADF emitters. Our calculations on natures of excited states indicate that the

M06-2X is the only functional which well reproduces the natures of excited states of TADF emitters under investigation.

✓ To further check the degree of overlap between electron and hole orbitals, we reported Φ_S indices computed at M06-2X/6-31+G(d,p), CAM-B3LYP/6-31+G(d,p) and ωB97XD/6-31+G(d,p) levels of theory. Our findings represent that the M06-2X/6-31+G(d,p) provides the correct degree of separation between electron and hole orbitals.

✓ Based on the results from nature of states analysis, we further modelled the ΔE_{ST} and SOC parameter with the M06-2X functional and observed that M06-2X well reproduces the experimental ΔE_{ST} data obtained from the literature and it represents reliable SOC values consistent with RISC processes.

Based on the findings from four descriptor analyses, we theoretically proposed a comprehensive methodological approach to the TADF design strategies. Moreover, via considering the effects of four descriptors, we learnt that the SOC parameter has the determinative role in TADF efficiency. Thus, targeted aim of the researchers interested in designing and synthesizing new TADF emitters should be optimizing the SOC involved in RISC process. Additionally, we further proposed the role of intermediate triplet states on TADF performance which should be taken into consideration in modelling photophysical properties of TADF emitters.

Conclusion

Through a systematic study of a large panel of potential TADF chromophores we have elucidated the reasons behind the performance of the different descriptors, which may be used to forecast RISC probability. Singlet/triplet gap, ΔE_{ST}, is usually associated with twisting angle and the presence of strong electron donating and withdrawing groups. The results obtained with M06-2X are reliable and consistent with experimental data. Additionally, we also observed a significant deviation of the twisting angles of TADF molecules between ground and triplet excited state equilibrium geometries.

The identification of ΔE_{ST} values for the states presenting the larger SOC, allows to identify RIC accessible channels and further supports the role of SOC as the most reliable descriptor of TADF performance. Indeed, for most of the studied cases, SOC is the determinant factor in determining the probability of RISC. Furthermore, as the electronic density reorganization seems fundamental to assure TADF, Φ_S indices have been explicitly considered. A good correlation has been observed with structural parameters, such as the twisting angles, or electronic properties, including ΔE_{ST} values, also coherently with previous reported trends.[117]

Oscillator strength may also be regarded as highly important, especially dictating luminescence efficiency and is strongly correlated with the geometric properties. Our results show that while designing new TADF emitters with favourable properties such as small ΔE_{ST} values and strong SOC, the geometrical features of the constituents should be carefully adjusted vanishing oscillator strengths. Therefore, instead of perfect orthogonal geometries, smaller torsions with moderate ΔE_{ST} values, strong SOC and strong oscillator strengths, will lead to more efficient TADF devices. To sum up, our calculations successfully explain the TADF performance of a wide range of donor and acceptor groups and their characteristic structural behavior, also highlighting useful and computationally efficient indicators. We also further analyzed the possible RISC paths and showed that RIC involving highest excited triplet states may play an important role in mediating RISC when leading to high SOC. Hence, ΔE_{ST}, oscillator strength, and SOC descriptors should be combined when performing computational screening and rational molecular design.

Author Contributions

Corresponding Authors

(Viktorya Aviyente) E-mail: aviye@boun.edu.tr

(Saron Catak) E-mail: saron.catak@boun.edu.tr

Conflicts of interest

There are no conflicts to declare.

Acknowledgements

Notes and references

1   C. W. Tang and S. A. Vanslyke, Organic electroluminescent diodes, *Appl. Phys. Lett.*, 1987, **51**, 913–915.

2   Q. Zhang, H. Kuwabara, W. J. Potscavage, S. Huang, Y. Hatae, T. Shibata and C. Adachi, Anthraquinone-based intramolecular charge-transfer compounds: Computational molecular design, thermally activated delayed fluorescence, and highly efficient red electroluminescence, *J. Am. Chem. Soc.*, 2014, **136**, 18070–18081.

3   H. Uoyama, K. Goushi, K. Shizu, H. Nomura and C. Adachi, Highly efficient organic light-emitting diodes from delayed fluorescence, *Nature*, 2012, **492**, 234–238.

4   R. H. Chien, C. T. Lai and J. L. Hong, Enhanced aggregation emission of vinyl polymer containing tetraphenylthiophene pendant group, *J. Phys. Chem. C*, 2011, **115**, 5958–5965.

5   D. Jacquemin and D. Escudero, The short device lifetimes of blue PhOLEDs: Insights into the photostability of blue Ir(III) complexes, *Chem. Sci.*, 2017, **8**, 7844–7850.

6   D. G. Congrave, B. H. Drummond, P. J. Conaghan, H. Francis, S. T. E. Jones, C. P. Grey, N. C. Greenham, D. Credgington and H. Bronstein, A Simple Molecular Design Strategy for Delayed Fluorescence toward 1000 nm, *J. Am. Chem. Soc.*, 2019, **141**, 18390–18394.

7   S. Izumi, H. F. Higginbotham, A. Nyga, P. Stachelek, N. Tohnai, P. de Silva, P. Data, Y. Takeda and S. Minakata, Thermally Activated Delayed Fluorescent Donor–Acceptor–Donor–Acceptor π-Conjugated Macrocycle for Organic Light-Emitting Diodes, *J. Am. Chem. Soc.*, 2020, **142**, 1482–1491.

8   M.-Y. Leung, M.-C. Tang, W.-L. Cheung, S.-L. Lai, M. Ng, M.-Y. Chan and V. Wing-Wah Yam, Thermally Stimulated Delayed Phosphorescence (TSDP)-Based Gold(III) Complexes of Tridentate Pyrazine-Containing Pincer Ligand with Wide Emission Color Tunability and Their Application in Organic Light-Emitting Devices, *J. Am. Chem. Soc.*, 2020, jacs.9b12136.

9   V. Jankus, P. Data, D. Graves, C. McGuinness, J. Santos, M. R. Bryce, F. B. Dias and A. P. Monkman, Highly efficient TADF OLEDs: How the emitter-host interaction controls both the excited state species and electrical properties of the devices to achieve near 100% triplet harvesting and high efficiency, *Adv. Funct. Mater.*, 2014, **24**, 6178–6186.

10   T. Serevičius, T. Nakagawa, M. C. Kuo, S. H. Cheng, K. T. Wong, C. H. Chang, R. C. Kwong, S. Xia and C. Adachi, Enhanced electroluminescence based on thermally activated delayed fluorescence from a carbazole-triazine derivative, *Phys. Chem. Chem. Phys.*, 2013, **15**, 15850–15855.

11   L. Zhan, Z. Chen, S. Gong, Y. Xiang, F. Ni, X. Zeng, G. Xie and C. Yang, A Simple Organic Molecule Realizing Simultaneous TADF, RTP, AIE, and Mechanoluminescence: Understanding the Mechanism Behind the Multifunctional Emitter, *Angew. Chemie - Int. Ed.*, 2019, **58**, 17651–17655.

12   K. Zheng, F. Ni, Z. Chen, C. Zhong and C. Yang, Polymorph-Dependent Thermally Activated Delayed Fluorescence Emitters: Understanding TADF from a Perspective of

Aggregation State, *Angew. Chemie - Int. Ed.*, 2019, 1–6.

13   B. S. Kim and J. Y. Lee, Engineering of mixed host for high external quantum efficiency above 25% in green thermally activated delayed fluorescence device, *Adv. Funct. Mater.*, 2014, **24**, 3970–3977.

14   Q. Zhang, S. Xu, M. Li, Y. Wang, N. Zhang, Y. Guan, M. Chen, C. F. Chen and H. Y. Hu, Rationally designed organelle-specific thermally activated delayed fluorescence small molecule organic probes for time-resolved biological applications, *Chem. Commun.*, 2019, **55**, 5639–5642.

15   X. Li, G. Baryshnikov, C. Deng, X. Bao, B. Wu, Y. Zhou, H. Ågren and L. Zhu, A three-dimensional ratiometric sensing strategy on unimolecular fluorescence–thermally activated delayed fluorescence dual emission, *Nat. Commun.*, 2019, **10**, 1–9.

16   C. M. Tonge and Z. M. Hudson, Interface-Dependent Aggregation-Induced Delayed Fluorescence in Bottlebrush Polymer Nanofibers, *J. Am. Chem. Soc.*, 2019, **141**, 13970–13976.

17   Y. J. Yu, X. Tang, H. T. Ge, Y. Yuan, Z. Q. Jiang and L. S. Liao, Fluorenone-based thermally activated delayed fluorescence materials for orange-red emission, *Org. Electron. physics, Mater. Appl.*, 2019, **73**, 240–246.

18   C. Wu, Y. Zhang, D. Ma and Q. Wang, Phthalonitrile-based bipolar host for efficient green to red phosphorescent and TADF OLEDs, *Dye. Pigment.*, 2020, **173**, 107895.

19   D. Chen, X. Cai, X. L. Li, Z. He, C. Cai, D. Chen and S. J. Su, Efficient solution-processed red all-fluorescent organic light-emitting diodes employing thermally activated delayed fluorescence materials as assistant hosts: Molecular design strategy and exciton dynamic analysis, *J. Mater. Chem. C*, 2017, **5**, 5223–5231.

20   Y. J. Yu, X. Tang, H. T. Ge, Y. Yuan, Z. Q. Jiang and L. S. Liao, Fluorenone-based thermally activated delayed fluorescence materials for orange-red emission, *Org. Electron. physics, Mater. Appl.*, 2019, **73**, 240–246.

21   J. H. Kim, J. H. Yun and J. Y. Lee, *Adv. Opt. Mater.*, 2018, 6.

22   M. Cekaviciute, J. Simokaitiene, D. Volyniuk, G. Sini and J. V. Grazulevicius, Arylfluorenyl-substituted metoxytriphenylamines as deep blue exciplex forming bipolar semiconductors for white and blue organic light emitting diodes, *Dye. Pigment.*, 2017, **140**, 187–202.

23   Q. Zhang, J. Li, K. Shizu, S. Huang, S. Hirata, H. Miyazaki and C. Adachi, Design of efficient thermally activated delayed fluorescence materials for pure blue organic light emitting diodes, *J. Am. Chem. Soc.*, 2012, **134**, 14706–14709.

24   P. Rajamalli, D. Rota Martir and E. Zysman-Colman, Pyridine-functionalized carbazole donor and benzophenone acceptor design for thermally activated delayed fluorescence emitters in blue organic light-emitting diodes, *J. Photonics Energy*, 2018, **8**, 1.

25   C. Fan, C. Duan, Y. Wei, D. Ding, H. Xu and W. Huang, Dibenzothiophene-Based Phosphine Oxide Host and Electron-Transporting Materials for Efficient Blue Thermally Activated Delayed Fluorescence Diodes through Compatibility Optimization, *Chem. Mater.*, 2015, **27**, 5131–5140.

26   S. Hirata, Y. Sakai, K. Masui, H. Tanaka, S. Y. Lee, H. Nomura, N. Nakamura, M. Yasumatsu, H. Nakanotani, Q. Zhang, K. Shizu, H. Miyazaki and C. Adachi, Highly efficient blue electroluminescence based on thermally activated delayed fluorescence, *Nat. Mater.*, 2015, **14**, 330–336.

27   T. Northey and T. J. Penfold, The intersystem crossing mechanism of an ultrapure blue organoboron emitter, *Org. Electron.*, 2018, **59**, 45–48.

28   T. T. Bui, F. Goubard, M. Ibrahim-Ouali, D. Gigmes and F. Dumur, *Beilstein J. Org. Chem.*, 2018, 14, 282–308.

29   J. R. Cha, C. W. Lee and M. S. Gong, Effect of increasing electron donor units for high-efficiency blue thermally activated delayed fluorescence, *Dye. Pigment.*, 2017, **140**, 399–406.

30   H. Nakanotani, T. Higuchi, T. Furukawa, K. Masui, K. Morimoto, M. Numata, H. Tanaka, Y. Sagara, T. Yasuda and C. Adachi, High-efficiency organic light-emitting diodes with fluorescent emitters, *Nat. Commun.*, 2014, **5**, 1–7.

31   S. Y. Lee, T. Yasuda, Y. S. Yang, Q. Zhang and C. Adachi, Luminous Butterflies: Efficient Exciton Harvesting by Benzophenone Derivatives for Full-Color Delayed Fluorescence OLEDs, *Angew. Chemie*, 2014, **126**, 6520–6524.

32   Y. Qi, Z. Wang, S. Hou and J. Yu, Color stable and highly efficient hybrid white organic light-emitting devices using heavily doped thermally activated delayed fluorescence and ultrathin non-doped phosphorescence layers, *Org. Electron. physics, Mater. Appl.*, 2017, **43**, 112–120.

33   K. Matsuo and T. Yasuda, Blue thermally activated delayed fluorescence emitters incorporating acridan analogues with heavy group 14 elements for high-efficiency doped and non-doped OLEDs, *Chem. Sci.*, 2019, **10**, 10687–10697.

34   S. Sohn, B. Hyun Koh, J. Y. Baek, H. Chan Byun, J. H. Lee, D. S. Shin, H. Ahn, H. K. Lee, J. Hwang, S. Jung and Y. H. Kim, Synthesis and characterization of diphenylamine derivative containing malononitrile for thermally activated delayed fluorescent emitter, *Dye. Pigment.*, 2017, **140**, 14–21.

35   Y. Gao, Q. Q. Pan, L. Zhao, Y. Geng, T. Su, T. Gao and Z. M. Su, Realizing performance improvement of blue thermally activated delayed fluorescence molecule DABNA by introducing substituents on the para-position of boron atom, *Chem. Phys. Lett.*, 2018, **701**, 98–102.

36   K. Wang, K. Liu, C. J. Zheng, Y. Z. Shi, K. Liang, M. Zhang, X. M. Ou and X. H. Zhang, A comparative study of carbazole-based thermally activated delayed fluorescence emitters with different steric hindrance, *J. Mater. Chem. C*, 2017, **5**, 4797–4803.

37   S. Feng, X. Guo and J. Zhang, An effective strategy for simply varying relative position of two carbazole groups in the thermally activated delayed fluorescence emitters to achieve deep-blue emission, *Spectrochim. Acta - Part A Mol. Biomol. Spectrosc.*, , DOI:10.1016/j.saa.2019.117564.

38   M. P. Gaj, C. Fuentes-Hernandez, Y. Zhang, S. R. Marder and B. Kippelen, Highly efficient Organic Light-Emitting Diodes from thermally activated delayed fluorescence using a sulfone-carbazole host material, *Org. Electron. physics, Mater. Appl.*, 2015, **16**, 109–112.

39   T. Hosokai, H. Nakanotani, S. Santou, H. Noda, Y. Nakayama and C. Adachi, TADF activation by solvent freezing: The role of nonradiative triplet decay and spin-orbit coupling in carbazole benzonitrile derivatives, *Synth. Met.*, 2019, **252**, 62–68.

40   T. Serevičius, T. Nakagawa, M. C. Kuo, S. H. Cheng, K. T. Wong, C. H. Chang, R. C. Kwong, S. Xia and C. Adachi, Enhanced electroluminescence based on thermally activated delayed fluorescence from a carbazole-triazine derivative, *Phys. Chem. Chem. Phys.*, 2013, **15**, 15850–15855.

41   B. Huang, Q. Qi, W. Jiang, J. Tang, Y. Liu, W. Fan, Z. Yin, F. Shi, X. Ban, H. Xu and Y. Sun, Thermally activated delayed fluorescence materials based on 3,6-di-tert-butyl-9-((phenylsulfonyl)phenyl)-9H-carbazoles, *Dye. Pigment.*, 2014, **111**, 135–144.

42   S. Y. Byeon, J. H. Kim and J. Y. Lee, CN-Modified Host Materials for Improved Efficiency and Lifetime in Blue Phosphorescent and Thermally Activated Delayed Fluorescent Organic Light-Emitting Diodes, *ACS Appl. Mater. Interfaces*, 2017, **9**, 13339–13346.

43   P. Rajamalli, N. Senthilkumar, P. Gandeepan, P. Y. Huang, M. J. Huang, C. Z. Ren-Wu, C. Y. Yang, M. J. Chiu, L. K. Chu, H. W. Lin and C. H. Cheng, A New Molecular Design Based on Thermally Activated Delayed Fluorescence for Highly Efficient Organic Light Emitting Diodes, *J. Am. Chem. Soc.*, 2016, **138**, 628–634.

44   L. Wang, J. Jin, W. Zhang, B. Pan, Z. Huang and S. Zhuang, Toward high efficiency green phosphorescent organic light-emitting diodes by fine tuning the charge transporting properties of 1,2,4-thiadiazole based hosts, *Org. Electron. physics, Mater. Appl.*, 2015, **16**, 177–185.

45   Y. J. Lien, T. C. Lin, C. C. Yang, Y. C. Chiang, C. H. Chang, S. H. Liu, Y. T. Chen, G. H. Lee, P. T. Chou, C. W. Lu and Y. Chi, First N-Borylated Emitters Displaying Highly Efficient Thermally Activated Delayed Fluorescence and High-Performance OLEDs, *ACS Appl. Mater. Interfaces*, 2017, **9**, 27090–27101.

46   H. Tanaka, K. Shizu, H. Miyazaki and C. Adachi, Efficient green thermally activated delayed fluorescence (TADF) from a phenoxazine-triphenyltriazine (PXZ-TRZ) derivative, *Chem. Commun.*, 2012, **48**, 11392–11394.

47   Y. Olivier, M. Moral, L. Muccioli and J. C. Sancho-García, Dynamic nature of excited states of donor-acceptor TADF materials for OLEDs: How theory can reveal structure-property relationships, *J. Mater. Chem. C*, 2017, **5**, 5718–5729.

48   K. Wu, T. Zhang, L. Zhan, C. Zhong, S. Gong, N. Jiang, Z. H. Lu and C. Yang, Optimizing Optoelectronic Properties of Pyrimidine-Based TADF Emitters by Changing the Substituent for Organic Light-Emitting Diodes with External Quantum Efficiency Close to 25 % and Slow Efficiency Roll-Off, *Chem. - A Eur. J.*, 2016, **22**, 10860–10866.

49   Y. Kitamoto, T. Namikawa, D. Ikemizu, Y. Miyata, T. Suzuki, H. Kita, T. Sato and S. Oi, Light blue and green thermally activated delayed fluorescence from 10H-phenoxaborin-derivatives and their application to organic light-emitting diodes, *J. Mater. Chem. C*, 2015, **3**, 9122–9130.

50   G. Jiang, F. Li, X. Kong, J. Fan, Y. Song, C. Wang and L. Lin, Suppression of aggregation caused quenching in U-shaped thermally activated delayed fluorescence molecules : Tert-butyl effect, *J. Lumin.*, 2019, 116899.

51   C. C. Tsai, W. C. Huang, H. Y. Chih, Y. C. Hsh, C. W. Liao, C. H. Lin, Y. X. Kang, C. H. Chang, Y. J. Chang and C. W. Lu, Efficient donor-acceptor-donor borylated compounds with extremely small ΔEST for thermally activated delayed fluorescence OLEDs, *Org. Electron.*, 2018, **63**, 166–174.

52   T. Northey and T. J. Penfold, The intersystem crossing mechanism of an ultrapure blue organoboron emitter, *Org. Electron.*, 2018, **59**, 45–48.

53   M. Mamada, G. Tian, H. Nakanotani, J. Su and C. Adachi, The Importance of Excited-State Energy Alignment for Efficient Exciplex Systems Based on a Study of Phenylpyridinato Boron Derivatives, *Angew. Chemie*, 2018, **130**, 12560–12564.

54   K. Suzuki, S. Kubo, K. Shizu, T. Fukushima, A. Wakamiya, Y. Murata, C. Adachi and H. Kaji, Triarylboron-Based Fluorescent Organic Light-Emitting Diodes with External Quantum Efficiencies Exceeding 20 %, *Angew. Chemie - Int. Ed.*, 2015, **54**, 15231–15235.

55   Y. J. Shiu, Y. T. Chen, W. K. Lee, C. C. Wu, T. C. Lin, S. H. Liu, P. T. Chou, C. W. Lu, I. C. Cheng, Y. J. Lien and Y. Chi, Efficient thermally activated delayed fluorescence of functional phenylpyridinato boron complexes and high performance organic light-emitting diodes, *J. Mater. Chem. C*, 2017, **5**, 1452–1462.

56   X. Liang, Z. P. Yan, H. B. Han, Z. G. Wu, Y. X. Zheng, H. Meng, J. L. Zuo and W. Huang, Peripheral Amplification of Multi-Resonance Induced Thermally Activated Delayed Fluorescence for Highly Efficient OLEDs, *Angew. Chemie - Int. Ed.*, 2018, **57**, 11316–11320.

57   Y. J. Shiu, Y. C. Cheng, W. L. Tsai, C. C. Wu, C. T. Chao, C. W. Lu, Y. Chi, Y. T. Chen, S. H. Liu and P. T. Chou, Pyridyl Pyrrolide Boron Complexes: The Facile Generation of Thermally Activated Delayed Fluorescence and Preparation of Organic Light-Emitting Diodes, *Angew. Chemie - Int. Ed.*, 2016, **55**, 3017–3021.

58   Y. Gao, Q. Q. Pan, L. Zhao, Y. Geng, T. Su, T. Gao and Z. M. Su, Realizing performance improvement of blue thermally activated delayed fluorescence molecule DABNA by introducing substituents on the para-position of boron atom, *Chem. Phys. Lett.*, 2018, **701**, 98–102.

59   S. Y. Lee, T. Yasuda, Y. S. Yang, Q. Zhang and C. Adachi, Luminous Butterflies: Efficient Exciton Harvesting by Benzophenone Derivatives for Full-Color Delayed Fluorescence OLEDs, *Angew. Chemie*, 2014, **126**, 6520–6524.

60   A. Tomkeviciene, T. Matulaitis, M. Guzauskas, V. Andruleviciene, D. Volyniuk and J. V. Grazulevicius, Thianthrene and acridan-substituted benzophenone or diphenylsulfone: Effect of triplet harvesting via TADF and phosphorescence on efficiency of all-organic OLEDS, *Org. Electron.*, 2019, **70**, 227–239.

61   S. Youn Lee, T. Yasuda, H. Nomura and C. Adachi, High-

efficiency organic light-emitting diodes utilizing thermally activated delayed fluorescence from triazine-based donor-acceptor hybrid molecules, *Appl. Phys. Lett.*, 2012, **101**, 9–13.

62   T. Hosokai, H. Matsuzaki, H. Nakanotani, K. Tokumaru, T. Tsutsui, A. Furube, K. Nasu, H. Nomura, M. Yahiro and C. Adachi, Evidence and mechanism of efficient thermally activated delayed fluorescence promoted by Delocalized Excited States, *Sci. Adv.*, 2017, **3**, 1–10.

63   Y. K. Wang, S. F. Wu, Y. Yuan, S. H. Li, M. K. Fung, L. S. Liao and Z. Q. Jiang, Donor-σ-Acceptor Molecules for Green Thermally Activated Delayed Fluorescence by Spatially Approaching Spiro Conformation, *Org. Lett.*, 2017, **19**, 3155–3158.

64   T. Nakagawa, S. Y. Ku, K. T. Wong and C. Adachi, Electroluminescence based on thermally activated delayed fluorescence generated by a spirobifluorene donor-acceptor structure, *Chem. Commun.*, 2012, **48**, 9580–9582.

65   D. S. M. Ravinson and M. E. Thompson, Thermally assisted delayed fluorescence (TADF): fluorescence delayed is fluorescence denied, *Mater. Horizons*, , DOI:10.1039/d0mh00276c.

66   Y. Olivier, J. C. Sancho-Garcia, L. Muccioli, G. D'Avino and D. Beljonne, Computational Design of Thermally Activated Delayed Fluorescence Materials: The Challenges Ahead, *J. Phys. Chem. Lett.*, 2018, **9**, 6149–6163.

67   S. Kothavale, W. J. Chung and J. Y. Lee, Color tuning of dibenzo[a , c]phenazine-2,7-dicarbonitrile-derived thermally activated delayed fluorescence emitters from yellow to deep-red , *J. Mater. Chem. C*, , DOI:10.1039/d0tc00960a.

68   F. B. Dias, J. Santos, D. R. Graves, P. Data, R. S. Nobuyasu, M. A. Fox, A. S. Batsanov, T. Palmeira, M. N. Berberan-Santos, M. R. Bryce and A. P. Monkman, The role of local triplet excited states and D-A relative orientation in thermally activated delayed fluorescence: Photophysics and devices, *Adv. Sci.*, 2016, **3**, 1–10.

69   I. Lyskov and C. M. Marian, Climbing up the ladder: Intermediate triplet states promote the reverse intersystem crossing in the efficient TADF emitter ACRSA, *J. Phys. Chem. C*, 2017, **121**, 21145–21153.

70   S. Xu, Q. Yang, Y. Wan, R. Chen, S. Wang, Y. Si, B. Yang, D. Liu, C. Zheng and W. Huang, Predicting intersystem crossing efficiencies of organic molecules for efficient thermally activated delayed fluorescence, *J. Mater. Chem. C*, 2019, **7**, 9523–9530.

71   M. Y. Wong and E. Zysman-Colman, Purely Organic Thermally Activated Delayed Fluorescence Materials for Organic Light-Emitting Diodes, *Adv. Mater.*, , DOI:10.1002/adma.201605444.

72   J. T. Ye, H. Q. Wang, Y. Zhang and Y. Q. Qiu, Regulation of the Molecular Architectures on Second-Order Nonlinear Optical Response and Thermally Activated Delayed Fluorescence Property: Homoconjugation and Twisted Donor-Acceptor, *J. Phys. Chem. C*, , DOI:10.1021/acs.jpcc.9b10067.

73   J. M. Mewes, Modeling TADF in organic emitters requires a careful consideration of the environment and going beyond the Franck-Condon approximation, *Phys. Chem. Chem. Phys.*, 2018, **20**, 12454–12469.

74   Y. H. Shi, F. Wang, M. Y. Sui, G. Y. Sun and Y. Z. Xie, Distinctly Diverse PLQY and Inverse Solid-State Luminescent Properties in Structure-Similar Diphenyl Sulfone TADF Molecules: A Role of C–C, *Adv. Theory Simulations*, 2020, **2000037**, 1–7.

75   E. E. Bas, P. Ulukan, A. Monari, V. Aviyente and S. Catak, Photophysical Properties of Benzophenone Based TADF Emitters in Relation to Their Molecular Structure, 2022, 1–14.

76   I. Frisch, M. J.; Trucks, G. W.; Schlegel, H. B.; Scuseria, G. E.; Robb, M. A.; Cheeseman, J. R.; Scalmani, G.; Barone, V.; Petersson, G. A.; Nakatsuji, H.; Li, X.; Caricato, M.; Marenich, A. V.; Bloino, J.; Janesko, B. G.; Gomperts, R.; Mennucci, B.; Hratch, Gaussian 16, Revision C.01.

77   B. Zhao, Z. Liu, Z. Wang, H. Zhang, J. Li, H. Wang, B. Xu, Y. Wu and W. Li, Structural design for highly efficient pure fluorescent warm WOLEDs by employing TADF molecule as blue emitter and exciplex donor, *Org. Electron.*, 2019, **73**, 1–6.

78   Y. Zhao and D. G. Truhlar, The M06 suite of density functionals for main group thermochemistry, thermochemical kinetics, noncovalent interactions, excited states, and transition elements: Two new functionals and systematic testing of four M06-class functionals and 12 other function, *Theor. Chem. Acc.*, 2008, **120**, 215–241.

79   D. Josa, J. Rodríguez-Otero, E. M. Cabaleiro-Lago and M. Rellán-Piñeiro, Analysis of the performance of DFT-D, M05-2X and M06-2X functionals for studying π···π interactions, *Chem. Phys. Lett.*, 2013, **557**, 170–175.

80   A. D. Becke, A new mixing of Hartree-Fock and local density-functional theories, *J. Chem. Phys.*, 1993, **98**, 1372–1377.

81   T. Yanai, D. P. Tew and N. C. Handy, A new hybrid exchange-correlation functional using the Coulomb-attenuating method (CAM-B3LYP), *Chem. Phys. Lett.*, 2004, **393**, 51–57.

82   B. Aslanoglu, I. Yakavets, V. Zorin, H. P. Lassalle, F. Ingrosso, A. Monari and S. Catak, Optical properties of photodynamic therapy drugs in different environments: The paradigmatic case of temoporfin, *Phys. Chem. Chem. Phys.*, 2020, **22**, 16956–16964.

83   A. Kolleth, S. Müller, A. Lumbroso, G. Tanriver, S. Catak, S. Sulzer-Mossé and A. De Mesmaeker, Access to 3-aminobenzothiophenes and 3-aminothiophenes fused to 5-membered heteroaromatic rings through 6π-electrocyclization reaction of keteniminium salts, *Tetrahedron Lett.*, 2018, **59**, 3242–3248.

84   A. Zabaradsti, A. Kakanejadifard and M. Ghasemian, Theoretical study of molecular interactions of phosphorus ylide with hypohalous acids HOF, HOCl and HOBr, *Comput. Theor. Chem.*, 2012, **989**, 1–6.

85   J. Tomasi and M. Persico, Molecular Interactions in Solution: An Overview of Methods Based on Continuous Distributions of the Solvent, *Chem. Rev.*, 1994, **94**, 2027–

2094.

86   C. Y. Legault, CYLview Visualization and analysis software for computational chemistry 1.0b.

87   M. J. G. Peach, M. J. Williamson and D. J. Tozer, Influence of triplet instabilities in TDDFT, *J. Chem. Theory Comput.*, 2011, **7**, 3578–3585.

88   J. P. Dahl and M. Springborg, The Morse oscillator in position space, momentum space, and phase space, *J. Chem. Phys.*, 1988, **88**, 4535–4547.

89   M. Barbatti, M. Ruckenbauer, F. Plasser, J. Pittner, G. Granucci, M. Persico and H. Lischka, Newton-X: A surface-hopping program for nonadiabatic molecular dynamics, *Wiley Interdiscip. Rev. Comput. Mol. Sci.*, 2014, **4**, 26–33.

90   R. Al-Saadon, C. Sutton and W. Yang, Accurate Treatment of Charge-Transfer Excitations and Thermally Activated Delayed Fluorescence Using the Particle-Particle Random Phase Approximation, *J. Chem. Theory Comput.*, 2018, **14**, 3196–3204.

91   S. Kossmann, B. Kirchner and F. Neese, Performance of modern density functional theory for the prediction of hyperfine structure: Meta-GGA and double hybrid functionals, *Mol. Phys.*, 2007, **105**, 2049–2071.

92   T. Etienne, X. Assfeld and A. Monari, New insight into the topology of excited states through detachment/attachment density matrices-based centroids of charge, *J. Chem. Theory Comput.*, 2014, **10**, 3906–3914.

93   T. Etienne, X. Assfeld and A. Monari, Toward a quantitative assessment of electronic transitions" charge-transfer character, *J. Chem. Theory Comput.*, 2014, **10**, 3896–3905.

94   M. D. Hanwell, D. E. Curtis, D. C. Lonie, T. Vandermeerschd, E. Zurek and G. R. Hutchison, Avogadro: An advanced semantic chemical editor, visualization, and analysis platform, *J. Cheminform.*, , DOI:10.1186/1758-2946-4-17.

95   G. te Velde, F. M. Bickelhaupt, E. J. Baerends, C. Fonseca Guerra, S. J. A. van Gisbergen, J. G. Snijders and T. Ziegler, Chemistry with ADF, *J. Comput. Chem.*, 2001, **22**, 931–967.

96   C. Fonseca Guerra, J. G. Snijders, G. Velde and E. J. Baerends, Regular article Towards an order- N DFT method, *Theor. Chem. Acc.*, 1998, **99**, 391–403.

97   E. Van Lenthe and E. J. Baerends, Optimized Slater-type basis sets for the elements 1-118, *J. Comput. Chem.*, 2003, **24**, 1142–1156.

98   M. Girardon, S. Parant, A. Monari, F. Dehez, C. Chipot, E. Rogalska, N. Canilho and A. Pasc, Triggering Tautomerization of Curcumin by Confinement into Liposomes, *ChemPhotoChem*, 2019, **3**, 1034–1041.

99   C. Duan, J. Li, C. Han, D. Ding, H. Yang, Y. Wei and H. Xu, Multi-dipolar Chromophores Featuring Phosphine Oxide as Joint Acceptor: A New Strategy toward High-Efficiency Blue Thermally Activated Delayed Fluorescence Dyes, *Chem. Mater.*, 2016, **28**, 5667–5679.

100 P. Data, P. Pander, M. Okazaki, Y. Takeda, S. Minakata and A. P. Monkman, Dibenzo[a,j]phenazine-Cored Donor-Acceptor-Donor Compounds as Green-to-Red/NIR Thermally Activated Delayed Fluorescence Organic Light Emitters, *Angew. Chemie - Int. Ed.*, 2016, **55**, 5739–5744.

101 Q. Zhang, H. Kuwabara, W. J. Potscavage, S. Huang, Y. Hatae, T. Shibata and C. Adachi, Anthraquinone-based intramolecular charge-transfer compounds: Computational molecular design, thermally activated delayed fluorescence, and highly efficient red electroluminescence, *J. Am. Chem. Soc.*, 2014, **136**, 18070–18081.

102 T. Takahashi, K. Shizu, T. Yasuda, K. Togashi and C. Adachi, Donor-acceptor-structured 1,4-diazatriphenylene derivatives exhibiting thermally activated delayed fluorescence: Design and synthesis, photophysical properties and OLED characteristics, *Sci. Technol. Adv. Mater.*, , DOI:10.1088/1468-6996/15/3/034202.

103 S. Wang, X. Yan, Z. Cheng, H. Zhang, Y. Liu and Y. Wang, Highly Efficient Near-Infrared Delayed Fluorescence Organic Light Emitting Diodes Using a Phenanthrene-Based Charge-Transfer Compound, *Angew. Chemie*, 2015, **127**, 13260–13264.

104 Q. Zhang, B. Li, S. Huang, H. Nomura, H. Tanaka and C. Adachi, Efficient blue organic light-emitting diodes employing thermally activated delayed fluorescence, *Nat. Photonics*, 2014, **8**, 326–332.

105 S. Y. Lee, T. Yasuda, Y. S. Yang, Q. Zhang and C. Adachi, Luminous butterflies: Efficient exciton harvesting by benzophenone derivatives for full-color delayed fluorescence OLEDs, *Angew. Chemie - Int. Ed.*, 2014, **53**, 6402–6406.

106 Y. Kitamoto, T. Namikawa, D. Ikemizu, Y. Miyata, T. Suzuki, H. Kita, T. Sato and S. Oi, Light blue and green thermally activated delayed fluorescence from 10H-phenoxaborin-derivatives and their application to organic light-emitting diodes, *J. Mater. Chem. C*, 2015, **3**, 9122–9130.

107 W. L. Tsai, M. H. Huang, W. K. Lee, Y. J. Hsu, K. C. Pan, Y. H. Huang, H. C. Ting, M. Sarma, Y. Y. Ho, H. C. Hu, C. C. Chen, M. T. Lee, K. T. Wong and C. C. Wu, A versatile thermally activated delayed fluorescence emitter for both highly efficient doped and non-doped organic light emitting devices, *Chem. Commun.*, 2015, **51**, 13662–13665.

108 H. Uoyama, K. Goushi, K. Shizu, H. Nomura and C. Adachi, Highly efficient organic light-emitting diodes from delayed fluorescence, *Nature*, 2012, **492**, 234–238.

109 S. Huang, Q. Zhang, Y. Shiota, T. Nakagawa, K. Kuwabara, K. Yoshizawa and C. Adachi, Computational prediction for singlet- and triplet-transition energies of charge-transfer compounds, *J. Chem. Theory Comput.*, 2013, **9**, 3872–3877.

110 B. Albert and N. Cedex, Version of Record: https://www.sciencedirect.com/science/article/pii/S01650 32720326483, 5–10.

111 T. J. Penfold, On predicting the excited-state properties of thermally activated delayed fluorescence emitters, *J. Phys. Chem. C*, 2015, **119**, 13535–13544.

112 P. K. Samanta, D. Kim, V. Coropceanu and J. L. Brédas, Up-Conversion Intersystem Crossing Rates in Organic Emitters for Thermally Activated Delayed Fluorescence: Impact of the Nature of Singlet vs Triplet Excited States, *J. Am. Chem. Soc.*, 2017, **139**, 4042–4051.

113 J. Gibson and T. J. Penfold, Nonadiabatic coupling reduces the activation energy in thermally activated delayed fluorescence, *Phys. Chem. Chem. Phys.*, 2017, **19**, 8428–

      8434.
114   C. M. Marian, Mechanism of the Triplet-to-Singlet
      Upconversion in the Assistant Dopant ACRXTN, *J. Phys.*
      Chem. C, 2016, **120**, 3715–3721.
115   J. Gibson, A. P. Monkman and T. J. Penfold, The Importance
      of Vibronic Coupling for Efficient Reverse Intersystem
      Crossing in Thermally Activated Delayed Fluorescence
      Molecules, *ChemPhysChem*, 2016, 2956–2961.
116   T. Ogiwara, Y. Wakikawa and T. Ikoma, Mechanism of
      intersystem crossing of thermally activated delayed
      fluorescence molecules, *J. Phys. Chem. A*, 2015, **119**, 3415–
      3418.
117   T. Etienne, H. Gattuso, C. Michaux, A. Monari, X. Assfeld
      and E. A. Perpète, Fluorene-imidazole dyes excited states
      from first-principles calculations—Topological insights,
      Theor. Chem. Acc., 2016, **135**, 1–11.